Journal of
Manufacturing and Materials Processing

MDPI

Article

Hybrid Manufacturing of Stiffening Grooves in Additive Deposited Thin Parts

Valentino A. M. Cristino [1], João P. M. Pragana [2], Ivo M. F. Bragança [3], Carlos M. A. Silva [2] and Paulo A. F. Martins [2,*]

[1] Department of Electromechanical Engineering, University of Macao, Avenida da Universidade, Taipa, Macao 999078, China; vcristino@umac.mo
[2] IDMEC, Instituto Superior Tecnico, Universidade de Lisboa, Av. Rovisco Pais, 1049-001 Lisboa, Portugal; joao.pragana@tecnico.ulisboa.pt (J.P.M.P.); carlos.alves.silva@tecnico.ulisboa.pt (C.M.A.S.)
[3] CIMOSM, Instituto Superior de Engenharia de Lisboa, Instituto Politécnico de Lisboa, 1959-007 Lisboa, Portugal; ivo.braganca@isel.pt
* Correspondence: pmartins@tecnico.ulisboa.pt

Abstract: This paper is focused on the hybridization of additive manufacturing with single-point incremental forming to produce stiffening grooves in thin metal parts. An analytical model built upon in-plane stretching of a membrane is provided to determine the tool force as a function of the required groove depth and to estimate the maximum allowable groove depth that can be formed without tearing. The results for additively deposited stainless-steel sheets show that the proposed analytical model can replicate incremental plastic deformation of the stiffening grooves in good agreement with experimental observations and measurements. Anisotropy and lower formability caused by the dendritic-based microstructure of the additively deposited stainless-steel sheets justifies the reason why the maximum allowable depth of the stiffening grooves is approximately 27% smaller than that obtained for the wrought commercial sheets of the same material that are used for comparison purposes.

Keywords: hybrid metal additive manufacturing; incremental forming; stiffening grooves; analytical modeling; experimentation

Citation: Cristino, V.A.M.; Pragana, J.P.M.; Bragança, I.M.F.; Silva, C.M.A.; Martins, P.A.F. Hybrid Manufacturing of Stiffening Grooves in Additive Deposited Thin Parts. *J. Manuf. Mater. Process.* **2021**, *5*, 140. https://doi.org/10.3390/jmmp5040140

Academic Editors: Marco Mandolini, Paolo Cicconi and Patrick Pradel

Received: 13 November 2021
Accepted: 18 December 2021
Published: 20 December 2021

1. Introduction

Stretching is a metal forming process in which an initially flat sheet, gripped along its edges, is stretched and bent simultaneously with the intention of obtaining a contoured panel by enlargement of the surface and reduction of thickness (Figure 1a). The process is widely used in aerospace, automotive, shipbuilding and civil construction for producing panels with various dimensions that, in some cases, may exceed 50 m^2 [1].

Strengthening the panels produced by stretching by means of individual stringers (Figure 1b) that are welded, riveted or rigidly fastened to their surfaces is a necessary and commonly used procedure to allow panels to withstandg the tension, compression, bending, shear and torsion efforts that may be applied to them in service.

The inverse approach of strengthening the panels with stringers before stretching is often limited by cracking and plastic instability (buckling) of the stringers and panels due to the tensile or compressive stresses that may be induced during the forming process. However, recent developments by Köhler et al. [2], who proposed a cam-actuated mechanism to provide lateral support of stringers during forming of the panels, show potential to make the inverse approach feasible even though the suppression of buckling may lead to new failure modes, higher amounts of spring back after forming and increased tooling costs when compared with the conventional stretching and strengthening approach.

An alternative to panels with stringers made from multiple parts that require assembly before or after forming is the fabrication of monolithic panels with integrated stringers

by milling, or by additive manufacturing on the surface of the already formed panels. Monolithic panels produced by milling are homogeneous, offer excellent strength-to-weight ratios and provide significant cost savings in assembly, labor and tooling. However, their application is limited by surface roughness, machining time, geometry accuracy and material wastage (typically, above 95% of the initial blank) [3,4]. These panels are mainly used in aerospace applications.

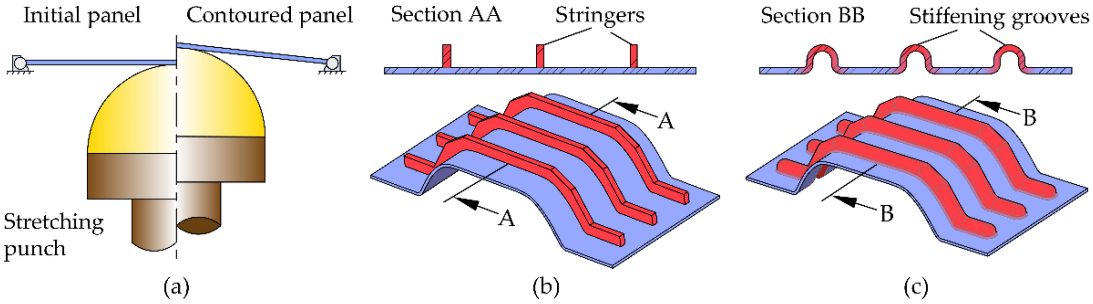

Figure 1. (**a**) Fabrication of sheet metal panels by stretching; strengthening of sheet metal panels by (**b**) longitudinal stringers and by (**c**) longitudinal stiffening grooves.

Direct manufacture of stringers through additive manufacturing has recently been proposed for the self-reinforcement of aircraft fuselage panels [5]. However, the advantages resulting from the elimination of assembling procedures with rivets or screws and the reduction in material waste when compared to monolithic panels fabricated by milling must be equated in view of the potential disadvantages resulting from the occurrence of heat-affected zones with metallurgical changes in the material of the panels and thermal-induced distortions that may compromise the final required geometry and performance of the panels.

Recent developments in incremental sheet metal forming processes opened the possibility of using single-point incremental forming (SPIF) to produce stiffening grooves in monolithic panels [6] (Figure 1c). Stiffening grooves are a special type of stringers that are produced by local pressing of the sheet panels during forming, and the possibility of carrying out forming and stiffening stages simultaneously, in a single-clamping operation, has the potential for great economic benefits. Moreover, the dieless characteristics of SPIF provides a level of flexibility much higher than that offered by the conventional forming of grooves with punch and die sets [7,8], which are panel and groove-shape dependent. Alternative solutions based on electromagnetic forming are groove-shape dependent and limited to highly conductive materials and to small geometries due to the available coil sizes [9].

The need for additional reinforcements is not exclusive to large panels because there are other thin metal parts of smaller dimensions that have bends in more than one plane which also need to be strengthened in order to withstand the efforts that are applied to them in service. This is particularly important in the case of lightweight additive manufactured parts, which require the use of support structures whenever complex out-of-plane-shaped features are to be included to preserve the overall geometric integrity of the parts, and prevent the occurrence of defects and failures, such as deformations, dross formation or warpage [10]. In such cases, it makes sense to investigate the possibility of implementing a new hybrid metal additive manufacturing approach [11] that combines additive manufacturing and in-plane stretching by SPIF to produce local, customized, stiffening grooves.

The term 'hybrid manufacturing' is hereafter used to designate a process sequence and is strongly associated to the gains of combining innovative manufacturing approaches instead of traditional manufacturing routes. This open definition of hybrid manufacturing [12] is different from the classical (narrow) definition in which two or more processes are combined in situ at the time and has been previously utilized in a process sequence

combining additive manufacturing, metal cutting and coining to fabricate collector coins with complex intricate contoured holes [13].

Under these circumstances, this paper is focused on the combination of wire-arc additive manufacturing (WAAM) and SPIF to produce stiffening grooves in thin metal parts. In a broader perspective, the work can also be seen as a first attempt to hybridize additive manufacturing with dieless incremental forming for the embossing of stiffeners, letters, numbers and decorative designs with moderate-to-high depths and thickness changes in the parts.

The work is performed in additively deposited stainless-steel sheets and includes a new analytical model to predict the force and the maximum admissible stiffening groove depth produced by SPIF. Wrought commercial stainless-steel sheets are included for comparison purposes and the overall results show that the proposed analytical model can be successfully used to characterize plastic deformation and failure by the tearing in hybrid additive manufacturing of stiffening grooves. Microstructure observations and anisotropy justify the differences in the mechanical response of the additively deposited and wrought commercial stainless-steel sheets, in agreement with previous observations of the authors in the same material [14] and of other authors in different materials [15].

2. Materials and Methods

2.1. Additively Deposited and Wrought Commercial Materials

Hybrid additive manufacturing of stiffening grooves was carried out in AISI 316L stainless-steel sheets deposited by WAAM in a 3-axis CNC system equipped with an ESAB LUC Aristo 400 gas metal arc welding machine. The material was supplied as a wire with 1-mm diameter through a welding torch and melted, at the time of deposition, onto a 260 × 70 × 15 (mm) hot-rolled AISI 316L baseplate (Figure 2a).

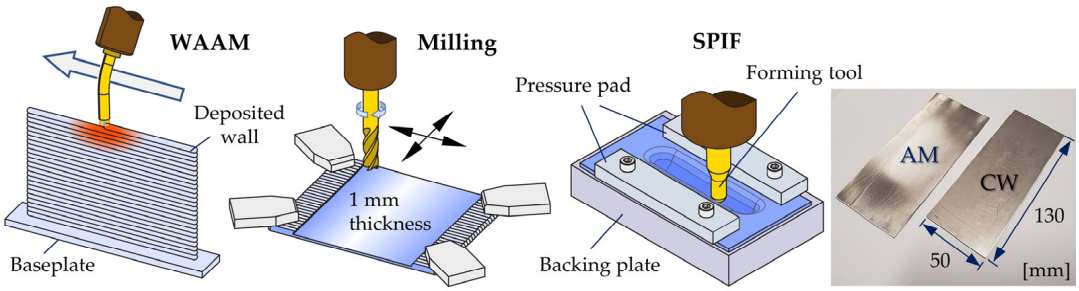

Figure 2. (**a**) Schematic representation of the hybrid manufacturing route to produce the AISI 316L stainless-steel sheets with stiffening grooves. (**b**) Photograph showing the additively manufactured and wrought commercial sheets before creating the stiffening grooves.

Deposition was carried out one layer at a time with a single bead and the torch was programmed with a reciprocate movement and a working angle of 90° to avoid concentrating the overlapped beads along the same edge of the built parts. The built parts consisted of walls with approximately 175 mm height, 200 mm width and 4 mm thickness and the main parameters utilized in material deposition are summarized in Table 1. Argon 99.9% was utilized as a shielding gas.

Table 1. Main parameters used in the deposition of AISI 316L stainless-steel by WAAM.

Current (A)	Voltage (V)	Wire Feed Speed (m/min)	Travel Speed (m/min)	Stick-Out Length (mm)	Gas Flow Rate (L/min)	Bead Height (mm)
100	16.5	6	0.6	10	10	1.8

After deposition, the built parts were milled and polished to match the dimensions and surface conditions of the wrought commercial AISI 316L sheets with 130 mm length, 50 mm width and 1 mm thickness that were used for comparison purposes (Figure 2b). The manufacturing route to produce the additively deposited sheets is schematically depicted in Figure 2a.

The flow curves of the additively deposited and wrought commercial AISI 316L stainless-steel sheets were determined by means of tensile tests on an INSTRON 5900 universal testing machine. The tests were carried out in accordance with the ASTM standard E8/E8 M-16 [16] and required cutting out specimens from the sheets at 0°(P-parallel), 45°(I-inclined) and 90°(T-transversal) inclination with respect to the build or rolling directions for each type of sheet. The results of these tests are shown in Figure 3, and Table 2 includes a summary of the mechanical properties for each testing direction.

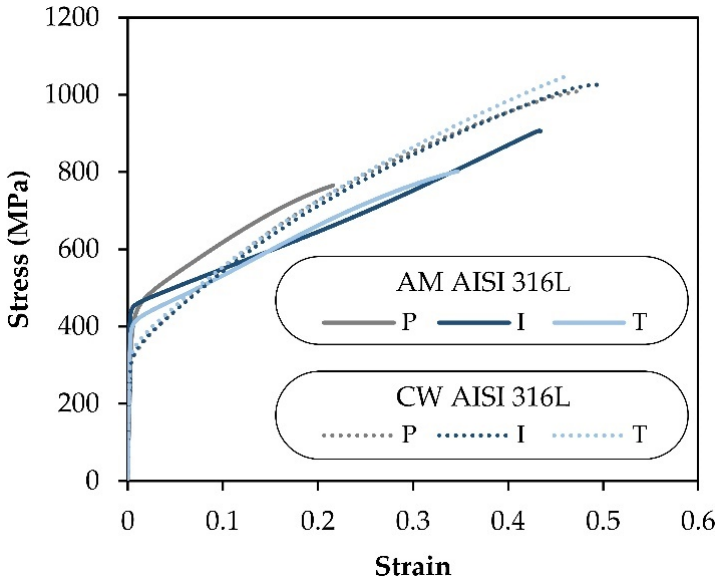

Figure 3. Flow stress of the additively deposited and wrought commercial AISI 316L stainless-steel sheets for the parallel (P), inclined (I) and transverse (T) directions with respect to the build or rolling directions, respectively.

Table 2. Mechanical properties of the additively deposited and wrought commercial AISI 316L stainless-steel sheets.

Material	Direction	Yield Stress (MPa)	Elongation at Break (%)	Anisotropy Coefficient
Additively deposited	P	395.6 ± 5.0	23.7 ± 5.1	0.81
	I	410.2 ± 5.5	54.5 ± 10.1	0.02
	T	392.5 ± 4.5	41.4 ± 9.8	3.35
Wrought commercial	P	320.7 ± 4.4	64.9 ± 3.3	0.94
	I	313.5 ± 3.1	63.6 ± 3.5	0.97
	T	310.5 ± 3.8	61.2 ± 4.1	0.98

The formability limits of the additively deposited and wrought commercial AISI 316L stainless-steel sheets were determined by combining the surface strains acquired by a digital image correlation (DIC) during tensile tests with measurements of the final thickness of the cracked surfaces with a stereomicroscope to obtain the gauge length strains at the fracture. The procedure is comprehensively explained in a previous paper published by the authors [14], from where the fracture forming limits (FFLs) of the two types of sheets that are shown in Figure 4 were retrieved.

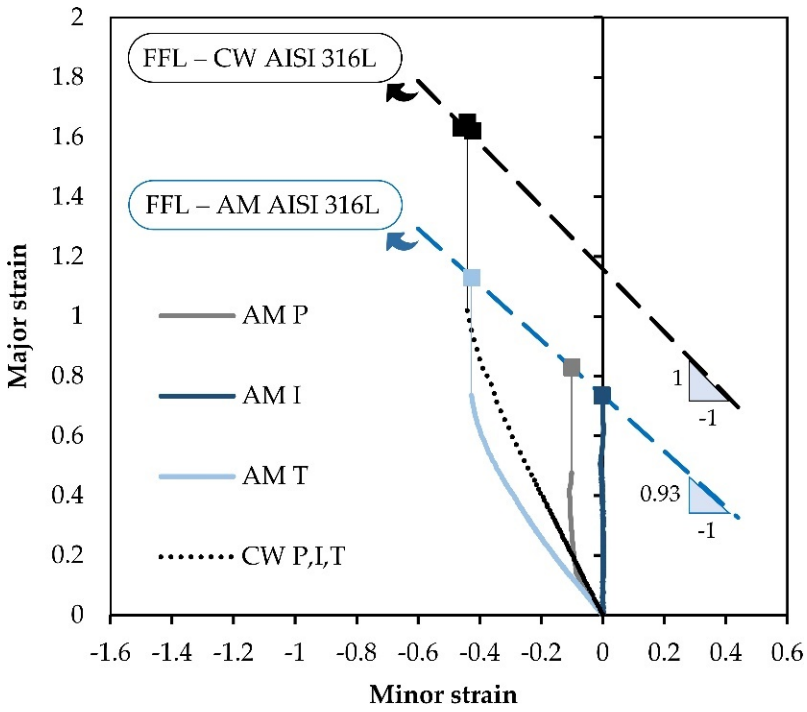

Figure 4. Fracture forming limits of the additively deposited and wrought commercial AISI 316L stainless-steel sheets in principal strain space (data obtained from [14]).

2.2. Single-Point Incremental Forming of the Stiffening Grooves

The additively deposited and wrought commercial AISI 316L stainless-steel sheets were placed in the experimental apparatus that is schematically shown in Figure 2a for producing the stiffening grooves (hereafter referred to simply as 'grooves') by single-point incremental forming. The main components of the apparatus are (a) the semi-hemispherical forming tool with a 12 mm diameter, (b) the backing plate with a slot width of 20 mm and (c) the screw-loaded pressure pad located at the outer perimeter of the blank to prevent the sheets from drawing-in.

The tool is made from a cold working alloy tool steel with chromium, vanadium and tungsten (120WV4—DIN), hardened and tempered to 60 HRC, and the tests were performed with a reciprocating straight tool path along the longitudinal direction and a vertical step size of 1 mm per tool path. The tool feed rate was set equal to 200 mm/min and the rotation of the tool was set to 100 rpm. A ceramic grease Weicon ASW 040P was applied on the tool–sheet contact interface.

Reciprocating straight tool paths to produce grooves with smaller lengths are often used to evaluate the tearing depth of wrought commercial sheets [6,17], but its use in additively deposited sheets has never been investigated as far as the authors are aware.

The experimental distribution of in-plane strains $(\varepsilon_\phi, \varepsilon_z)$ on the surface of the grooves was determined by a circle grid analysis (CGA). For this purpose, a grid of overlapping circles with a 2 mm initial diameter was electrochemically etched on the sheets and the major and minor axis of the ellipses that resulted from plastic deformation of the circles were measured in various groove configurations corresponding to different depths H (Figure 5). The measurements were performed with a computer-aided system consisting of a 3Com USB camera and the GPA 3.0 software.

Assuming that stretching of the grooves by single-point incremental forming is carried out under proportional strain loading paths with a slope $\beta = d\varepsilon_z/d\varepsilon_\phi = 0$, as will be shown later in Section 3, and making use of the Hill's 48 anisotropic yield criterion [18] under plane stress $\sigma_t = 0$ conditions along the thickness direction, the experimental distribution

of effective strain $\bar{\varepsilon}$ along the perimeter of the groove can be obtained from the circle grid measurements of meridional strain ε_ϕ, as follows:

$$\bar{\varepsilon} = \sqrt{\frac{2}{3}\frac{(2+r)(1+r)}{(1+2r)}}\varepsilon_\phi \tag{1}$$

where $r = 1/4(r_0 + 2r_{45} + r_{90})$ is the normal anisotropy.

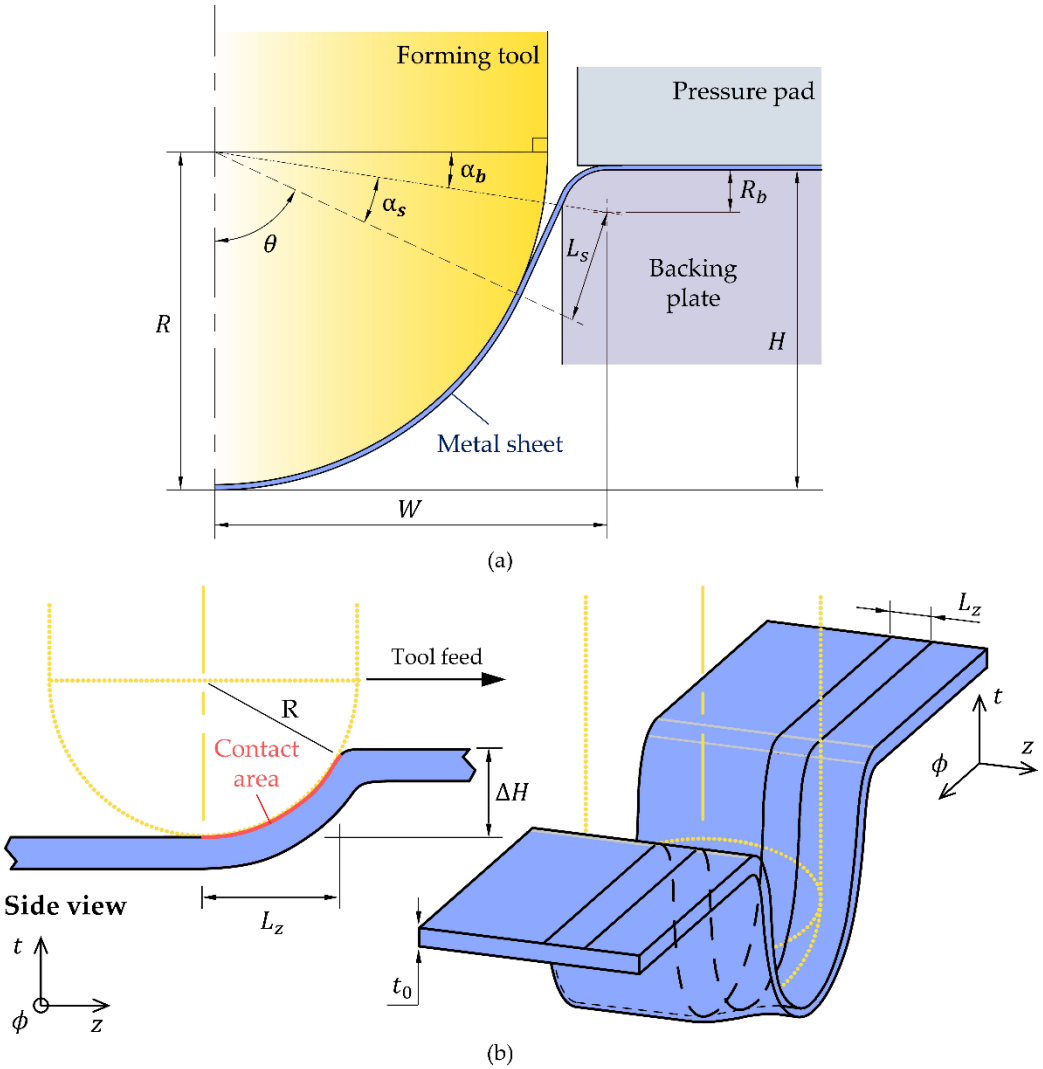

Figure 5. (**a**) Schematic representation of the stiffening groove with main notation; (**b**) schematic representation of the area corresponding to the local contact between the tool and the sheet placed immediately ahead (z-direction).

The result obtained in (1) allows for determining the experimental distributions of effective $\overline{\sigma}$ stress (assuming a Ludwik–Hollomon strain-hardening relationship), and meridional σ_ϕ stress, as indicated,

$$\begin{aligned} \overline{\sigma} &= k\bar{\varepsilon}^n \\ \sigma_\phi &= \sqrt{\tfrac{2}{3}(1+r)}\,\overline{\sigma} \end{aligned} \tag{2}$$

2.3. Analytical Model for the Incremental Forming of the Stiffening Grooves

The stiffening grooves are incrementally formed under plane strain deformation conditions. There is an exception to this type of material flow at the beginning of the

process during which the tool is vertically pressed against the sheet such as in biaxial stretching with a semi-hemispherical punch. However, the beginning of the process will be left out of the model and the derivation is only valid for steady-state material flow conditions.

A typical cross-section of the groove is approximated by a shell with three-main regions corresponding to (i) the wrap angle θ around the semi-hemispherical tool, (ii) the straight unsupported surface with a length L_s making an angle α_s with the tool center and (iii) the curvature radius R_b at the transition between the undeformed and the plastically deformed material. These regions and associated notation are schematically shown in Figure 5a, where the symbol R denotes the radius of the tool and the symbols H and W are the depth and half-width of the groove, respectively.

The shell is assumed as a membrane so that bending moments are neglected (i.e., the forces are essentially transmitted through the sheet surfaces subjected to in-plane stretching), and the meridional (ϕ), thickness (t) and longitudinal (z) directions are assumed as principal directions. Further simplifications in the model consider the material to be (i) rigid-plastic (i.e., no elastic effects are included) and (ii) anisotropic, following the Hill's 48 yield criterion [18] under plane stress conditions ($\sigma_t \cong 0$). Moreover, it is presumed that material strain hardening tends to balance the reduction in thickness so that the force per unit of length $T_\phi = \sigma_\phi t$ in the meridional direction can be assumed as constant. This last assumption is commonly used in the membrane analysis of sheet metal forming processes [19].

The presentation of the analytical model is subdivided into two parts; firstly, the authors focus on the calculation of the tool force F by modification of an earlier model developed by Martins and Marques [20] for conventional stretching with a cylindrical punch. Secondly, the authors explain the procedure to determine the maximum allowable groove depth H without tearing, taking into consideration the material formability limits (Section 2.2).

2.3.1. Tool Force

From Figure 5, the wrap angle θ around the semi-hemispherical tool can be written as follows:

$$\theta = \frac{\pi}{2} - \alpha_s - \alpha_b \tag{3}$$

where the angles α_s and α_b of the straight unsupported surface and of the transition between the undeformed and the plastically deformed material are related to H and W of the groove, in the following way:

$$\alpha_b = arctan\left(\frac{R - H + R_b}{W}\right) \tag{4}$$

$$\alpha_s = arccos\left(\frac{R_b + R}{\sqrt{\left\{W^2 + (R - H + R_b)^2\right\}}}\right) \tag{5}$$

The half-perimeter of the groove L_ϕ for an arbitrary depth H is given by

$$L_\phi = (R + R_b)\theta + L_s \tag{6}$$

where the length L_s of straight unsupported groove surface is determined from

$$L_s = \sqrt{\{W - (R + R_b)sin\theta\}^2 + \{H - (R + R_b)(1 - cos\theta)\}^2} \tag{7}$$

Once the half-perimeter L_ϕ of the groove is known, the average value of the meridional strain ε_ϕ^{avg} is obtained from

$$\varepsilon_\phi^{avg} = ln\left(\frac{L_\phi}{W}\right) \tag{8}$$

and the force F applied by the tool is written as

$$F = 2\sigma_{\phi}^{avg} t_0 L_z sin\theta exp\left(-\varepsilon_{\phi}^{avg}\right) \tag{9}$$

In the above equation, the symbol t_0 is the undeformed sheet thickness, L_z is the contact length in the z-direction (Figure 5b) and σ_{ϕ}^{avg} is the average meridional stress. The latter is obtained from the increments of average meridional strain $d\varepsilon_{\phi}^{avg}$ within successive configurations (under plane stress conditions along the thickness direction $\sigma_t = 0$) as follows:

$$\sigma_{\phi}^{avg} = \frac{\overline{\sigma}}{d\overline{\varepsilon}} \frac{(1+r)^2}{(1+2r)} d\varepsilon_{\phi}^{avg} \tag{10}$$

2.3.2. Maximum Allowable Depth

Merging the average meridional strain ε_{ϕ}^{avg} given by (8) with the constitutive equations relating the increments of strain with the applied stresses under combined plane strain ($\varepsilon_z = 0$) and plane stress ($\sigma_t = 0$) deformation conditions,

$$\begin{array}{c} d\varepsilon_{\phi} = \frac{d\overline{\varepsilon}}{\overline{\sigma}}\left(\frac{1}{1+r}\right)\left[\sigma_{\phi} + r\left(\sigma_{\phi} - \sigma_z\right)\right] \\ d\varepsilon_z = \frac{d\overline{\varepsilon}}{\overline{\sigma}}\left(\frac{1}{1+r}\right)\left[\sigma_z + r\left(\sigma_z - \sigma_{\phi}\right)\right] = 0 \\ d\varepsilon_t = \frac{d\overline{\varepsilon}}{\overline{\sigma}}\left(\frac{1}{1+r}\right)\left[-\sigma_z - \sigma_{\phi}\right] \end{array} \tag{11}$$

allows for writing the average distributions of thickness strain ε_t^{avg} and longitudinal stress σ_z^{avg} for an arbitrary groove depth H as follows:

$$\varepsilon_t^{avg} = -\varepsilon_{\phi}^{avg} \tag{12}$$

$$\sigma_z^{avg} = \frac{r}{1+r}\sigma_{\phi}^{avg} \tag{13}$$

The average thickness t^{avg} of the groove is then obtained from (12),

$$t^{avg} = t_0 exp\left(-\varepsilon_t^{avg}\right) \tag{14}$$

Having determined the average thickness t^{avg} and the average meridional stress σ_{ϕ}^{avg} directly from the analytical model, it is possible to obtain the force per unit of length T_{ϕ} that is assumed to have a constant value C for each groove depth H as follows:

$$T_{\phi} = t^{avg}\sigma_{\phi}^{avg} = C \tag{15}$$

By determining the critical meridional strain $\varepsilon_{\phi}^{crit}$ under plane strain deformation conditions through the intersection of the FFL with the vertical axis of Figure 4, and subsequently obtaining the critical meridional stress σ_{ϕ}^{crit} by replacement of the average values by the critical values in Equation (10), and identifying the minimum thickness t_{min} under the limiting material formability conditions of

$$t_{min} = t_0 exp\left(-\varepsilon_t^{crit}\right) \qquad \varepsilon_t^{crit} = -\varepsilon_{\phi}^{crit}, \tag{16}$$

it is possible to estimate the critical force per unit of length T_{ϕ}^{crit} as follows:

$$T_{\phi}^{crit} = t_{min}\sigma_{\phi}^{crit} = C^{crit} \tag{17}$$

This last result allows for obtaining the maximum allowable depth H_{max} by searching for the groove geometry that provides a force per unit of length T_{ϕ} (15) equal to the critical value C^{crit} at the onset of failure by fracture (17).

3. Results and Discussion

3.1. Strain Paths

Figure 6 shows the experimentally measured strains along the perimeter of the grooves produced along the parallel (P), inclined (I) and transverse (T) directions with respect to the build or rolling directions for the additively deposited and wrought commercial AISI 316L stainless-steel sheets. The results were obtained for the instant of time immediately after tearing by crack opening and propagation along the longitudinal direction (i.e., tool feed direction).

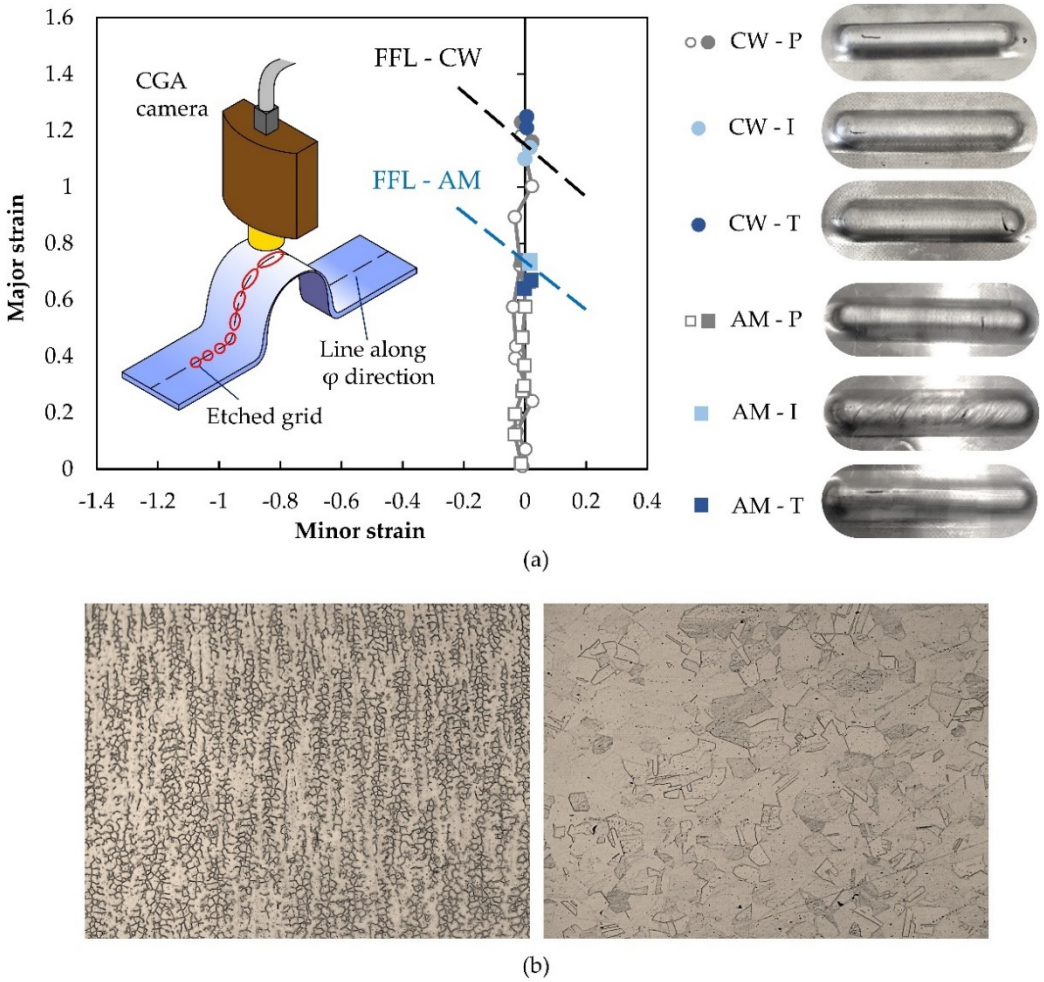

Figure 6. (**a**) Principal strain space showing the experimental strains that were measured by circle grid analysis in both additively deposited and wrought commercial sheets with photographs, showing details of the test specimens; (**b**) microstructures of metallographic samples taken from the (**left**) additively deposited and (**right**) wrought commercial AISI 316L stainless-steel sheets.

As seen, all of the strains lie close to the vertical axis, in agreement with the assumptions of the material being subjected to plane strain deformation under linear strain loading paths (refer to Sections 2.2 and 2.3). Moreover, the maximum strain values obtained from the circle grid analysis are also close to the FFLs of both additively deposited and wrought commercial sheets (Section 2.1), which are plotted as dashed straight lines falling from right to left in principal strain space. This last result, obtained for the two types of sheets, allows for concluding that incremental forming of the grooves fails by critical thickness reduction without previous necking in close agreement with crack opening by tension (mode I of fracture mechanics) [21].

Observation of the photographs included in Figure 6a reveals that the surface of the grooves that were incrementally formed along the inclined direction of the additively

deposited sheets contain a series of striations that coincide with the building direction (approximately 45° to the inclined direction). This type of texture is not visible in the corresponding specimen of the wrought commercial sheets and is attributed to the dendritic-based microstructure of the additively deposited sheets, which is made of columnar grains with primary arms aligned with the building direction and secondary arms bonding the neighboring grains together (Figure 6b). This type of microstructure, which was previously observed by the authors in tensile tests [14], is different from the equiaxial microstructure of the wrought commercial sheets and is the main reason behind the anisotropic behavior of the additively deposited sheets.

The last conclusion to be taken from Figure 6 is that, despite the differences in the surface texture of the grooves produced along the inclined direction of the additively deposited sheets, the strains at the fracture are close to those obtained for the other grooves produced along the parallel or transverse directions. Therefore, in what follows, there will be no distinction between the results obtained from each specific groove direction.

3.2. Maximum Allowable Depths

Figure 7 shows the theoretical evolution of the force per unit of length $T_\phi = t^{avg}\sigma_\phi^{avg}$ (15) with the groove depth H for materials following a Ludwik–Hollomon strain-hardening relationship $\overline{\sigma} = k\overline{\varepsilon}^n$, but having different values of the strain-hardening exponent n. To facilitate the comparison, it was decided to normalize the force per unit of length as follows:

$$\widetilde{T}_\phi = t^{avg}\frac{\sigma_\phi^{avg}}{k} \text{ with } \frac{\sigma_\phi^{avg}}{k} = \sqrt{\frac{2}{3}(1+r)}\,\frac{\overline{\sigma}^{avg}}{k} \tag{18}$$

where k is the constant of the Ludwik–Hollomon strain-hardening relationship.

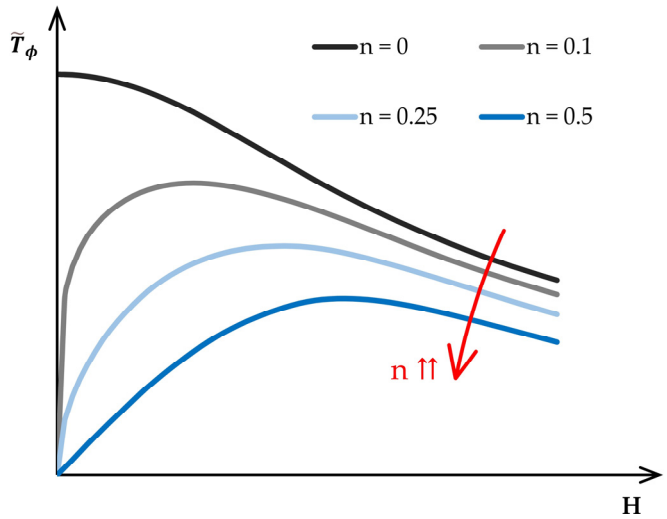

Figure 7. Influence of material strain hardening on the evolution of the normalized force per unit of length with the groove depth.

As seen, the evolution of the normalized force per unit of length is very much influenced by the strain-hardening exponent n, with peak values moving towards the vertical axis as the stress–strain response approaches that of a perfectly rigid–plastic material. In fact, when $n = 0$, the peak in the normalized force per unit of length occurs at the beginning of the process ($H = 0$) because there is no material strain hardening to compensate the reduction in thickness that is inherent to the incremental forming process, and the normalized force per unit of length falls monotonically from left to right as the thickness decreases with the groove depth H.

Increasing the strain-hardening exponent n gives rise to evolutions of the normalized force per unit of length with growth and decay regions separated by a peak value. This

means that strain hardening prevails at the beginning of the incremental forming process, whereas a reduction in thickness eventually leading to fracture prevails at the end of the process. The practical consequence of what was just said is that the identification of the maximum allowable depth H_{max} by searching the force per unit of length value C (15) that matches the critical value C^{crit} at the onset of failure by fracture (17) must only consider the decaying regions of the evolutions.

Transposition of above conclusion to the results obtained for the additively deposited and wrought commercial sheets that are depicted in Figure 8 results in the rightmost intersections between the dashed horizontal lines corresponding to the critical values C^{crit} at the onset of failure by fracture (17) and the force per unit of length evolution that is shown in the figure. The possible intersections on the left-growing evolution of the force per unit of length are discharged.

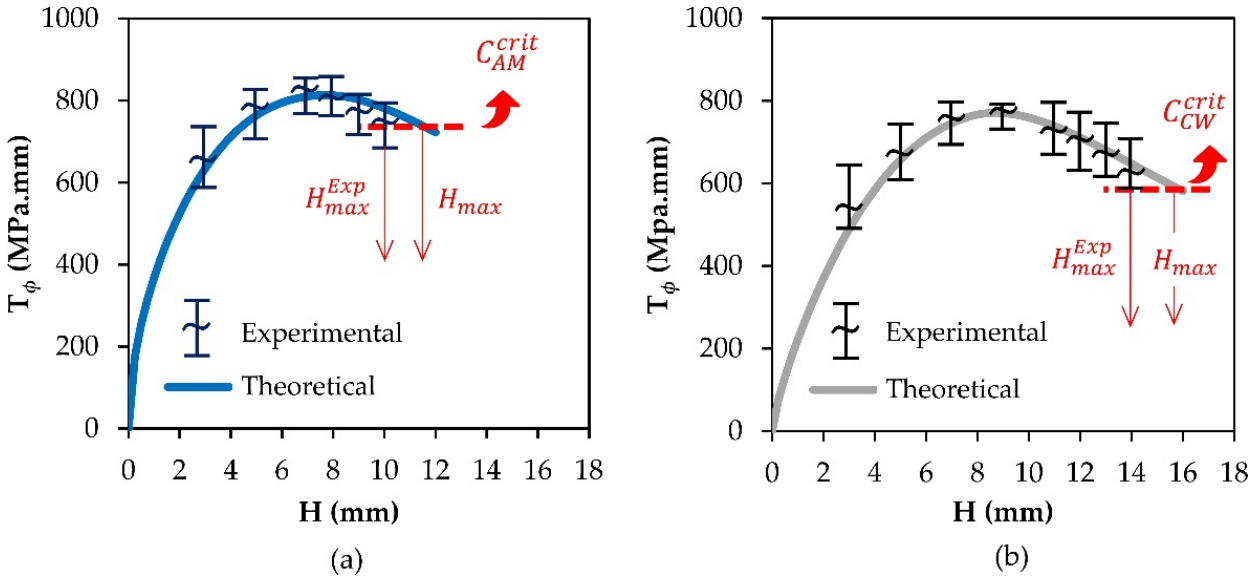

Figure 8. Evolution of the force per unit of length with the groove depth for the (**a**) additively deposited and (**b**) wrought commercial AISI 316L stainless-steel sheets. The dashed horizontal lines in both graphics correspond to the critical values and the intersections provide the maximum allowable predicted depths H_{max}.

The maximum allowable predicted depths H_{max} resulting from the above-mentioned intersections correspond to an overestimation of the maximum allowable experimental depths H_{max}^{Exp} below 20%. The experimental points included in Figure 8 serve only to validate the theoretical evolutions of the force per unit of length with the groove depth.

3.3. Tool Forces

Figure 9 presents the experimental and analytical evolutions of the tool force with the groove depth for the two different types of sheets. As seen, the analytical predicted evolution can replicate the overall trend of the experiments results but with a slight underestimation of the real values. The discrepancies are attributed to the overall assumptions of the analytical model, namely to the utilization of average instead of local values of the main variables, but also to some degree of uncertainty in defining the contact length L_z in the z-direction (Figure 5), because it may include a part of the tool surface located behind the vertical symmetry axis.

Scattering of the experimental data is larger for the additively deposited sheets due to anisotropy and, consequently, to different stress–strain responses during the tests performed along different directions with respect to the build direction. In connection to this, it is worth remembering that wrought commercial sheets are roughly isotropic ($r \approx 0.97$).

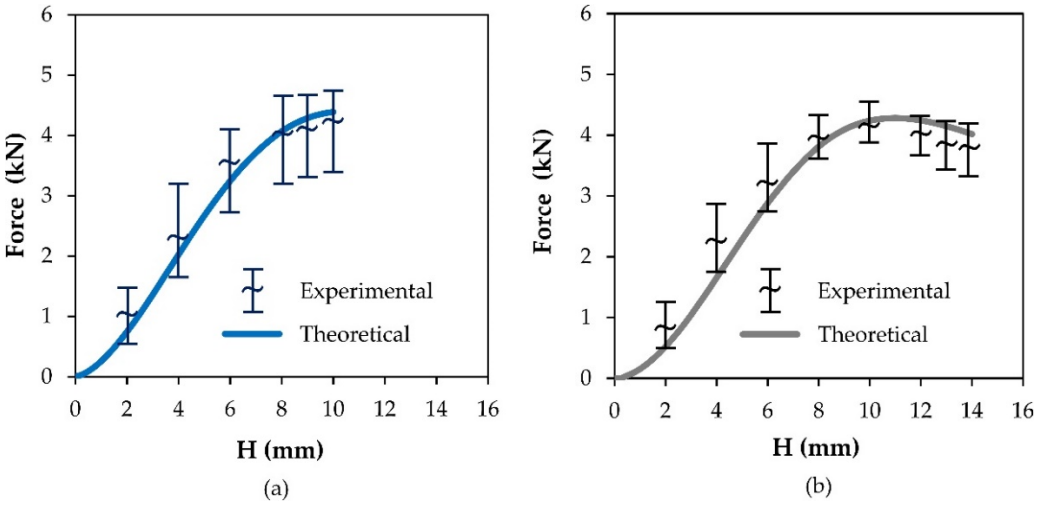

Figure 9. Evolution of the tool force with groove depth for the (**a**) additively deposited and (**b**) wrought commercial AISI 316L stainless-steel sheets.

All in all, the results show that a relatively simple analytical model based on a shell subjected to in-plane stretching can provide a good estimate of the tool forces.

4. Conclusions

Hybridization of additive manufacturing with single-point incremental forming can be utilized to produce stiffening grooves in thin sheets to improve their strength to withstand the efforts that are applied to them in service. Because out-of-plane grooves are not produced during material deposition, there is no need for using support structures to preserve the overall geometric integrity of the parts.

The estimates of the required force to produce a specific groove depth and of the maximum allowable groove depth that can be formed without tearing by means of a simple analytical model developed by the authors are in good agreement with the experimental observations and measurements. In particular, the results show that the maximum allowable stiffening grooves that can be produced in additively deposited AISI 316L stainless-steel sheets are approximately 27% smaller than those produced in wrought commercial AISI 316L stainless-steel sheets. This is due to anisotropy and to the lower formability induced by the dendritic-based microstructures resulting from the growth of grains along the temperature gradient during the heating–cooling cycles of material deposition.

Despite the above said disadvantages and limitations, the production of stiffening grooves in additively deposited thin sheets is interesting and feasible because grooves can undergo large plastic deformation before tearing.

Finally, it is worth mentioning that hybridization of additive manufacturing with single-point incremental forming to produce stiffening grooves can also be used in tubes, profiles and complex three-dimensional thin structures to improve their capability to withstand the different efforts that are applied to them in service.

Author Contributions: Conceptualization, C.M.A.S. and P.A.F.M.; methodology, V.A.M.C. and C.M.A.S.; software, C.M.A.S.; validation, V.A.M.C. and C.M.A.S.; formal analysis, C.M.A.S. and P.A.F.M..; investigation, V.A.M.C., J.P.M.P., I.M.F.B. and C.M.A.S.; resources, J.P.M.P., I.M.F.B. and C.M.A.S.; writing—original draft preparation, P.A.F.M.; writing—review and editing, V.A.M.C., J.P.M.P., I.M.F.B., C.M.A.S. and P.A.F.M.; visualization, V.C. and J.P.M.P.; supervision, C.M.A.S. and P.A.F.M.; project administration, P.A.F.M.; funding acquisition, V.A.M.C. and P.A.F.M. All authors have read and agreed to the published version of the manuscript.

Funding: This research was funded by Fundação para a Ciência e a Tecnologia of Portugal and IDMEC under LAETA-UIDB/50022/2020 and by the University of Macao through the start-up research grant (SRG2019-00161-FST).

Data Availability Statement: All the data supporting the reported results are available in the paper.

Acknowledgments: The authors would like to thank the support provided by Fundação para a Ciência e a Tecnologia of Portugal and IDMEC under LAETA-UIDB/50022/2020. Valentino Cristino would like to thank the support of the University of Macao through the start-up research grant (SRG2019-00161-FST).

Conflicts of Interest: The authors declare no conflict of interest.

References

1. Klocke, F. *Manufacturing Processes 4—Forming*; Springer: Aachen, Germany, 2013; pp. 332–339.
2. Köhler, S.; Rohnert, C.; Groche, P. Extension of geometric limits in drawing of stringer sheets. In Proceedings of the 17th International Conference on Metal Forming—Metal Forming 2018, Toyohashi, Japan, 16–19 September 2018; Mori, K.I., Abe, Y., Maeno, T., Eds.; Procedia Manufacturing: Amsterdam, Netherlands, 2018; Volume 15, pp. 693–700.
3. Seguy, S.; Campa, F.J.; Lacalle, L.N.L.; Arnaud, L.; Dessein, G.; Aramendi, G. Toolpath dependent stability lobes for the milling of thin-walled parts. *Int. J. Mach. Mach. Mater.* **2009**, *4*, 377–392. [CrossRef]
4. Shamsuddin, K.A.; Ab-Kadir, A.R.; Osman, M.H. A comparison of milling cutting path strategies for thin-walled aluminium alloys fabrication. *Int. J. Eng. Sci.* **2013**, *2*, 1–8.
5. World Premiere for Additive Manufacturing: STELIA Aerospace Presents a Demonstrator for Metallic Self-Reinforced Fuselage Panels Manufactured by 3D Impression. Available online: https://additivemanufacturing.com/2018/02/21/world-premiere-for-additive-manufacturing-stelia-aerospace-presents-a-demonstrator-for-metallic-self-reinforced-fuselage-pannels-manufactured-by-3d-impression/ (accessed on 15 February 2018).
6. Slota, J.; Kubit, A.; Trzepiecinski, T.; Krasowski, B.; Varga, J. Ultimate load-carrying ability of rib-stiffened 2024-T3 and 7075-T6 aluminium alloy panels under axial compression. *Materials* **2021**, *14*, 1176. [CrossRef] [PubMed]
7. Fusano, L.; Priarone, P.C.; Avalle, M.; Filippi, A.M. Sheet metal plate design: A structured approach to product optimization in the presence of technological constraints. *Int. J. Adv. Manuf. Technol.* **2011**, *56*, 31–45. [CrossRef]
8. Lacki, P.; Adamus, J. Numerical analysis of forming sheet panels with stiffening ribs. In Proceedings of the 13rd International Conference on Computational Plasticity. Fundamentals and Applications—COMPLAS XIII, Barcelona, Spain, 1–3 September 2015; pp. 204–215.
9. Eguia, I.; Mangas, A.; Iturbe, R.; Gutiérrez, M.A. Electromagnetic forming of longitudinal strengthening ribs in roll formed automotive profiles. In Proceedings of the 4th International Conference on High-Speed Forming—ICHSF 2010, Columbus, OH, USA, 9–10 March 2010; pp. 200–207.
10. Pragana, J.M.P.; Bragança, I.M.F.; Silva, C.M.A.; Martins, P.A.F. Integration of tube end forming in wire arc additive manufacturing: An experimental and numerical investigation. *Int. J. Adv. Manuf. Technol.* **2021**, *117*, 2715–2726. [CrossRef]
11. Pragana, J.M.P.; Sampaio, R.F.V.; Bragança, I.M.F.; Silva, C.M.A.; Martins, P.A.F. Hybrid metal additive manufacturing: A state–of–the-art review. *Adv. Ind. Manuf. Eng.* **2021**, *2*, 100032. [CrossRef]
12. Zhu, Z.; Dhokia, V.G.; Nassehi, A.; Newman, S.T. A review of hybrid manufacturing processes–state of the art and future perspectives. *Int. J. Comput. Integr. Manuf.* **2013**, *26*, 596–615. [CrossRef]
13. Pragana, J.P.M.; Rosenthal, S.; Bragança, I.M.F.; Silva, C.M.A.; Tekkaya, A.E.; Martins, P.A.F. Hybrid additive manufacturing of collector coins. *J. Manuf. Mater. Process.* **2020**, *4*, 115. [CrossRef]
14. Pragana, J.P.M.; Bragança, I.M.C.; Reis, L.; Silva, C.M.A.; Martins, P.A.F. Formability of wire-arc deposited AISI 316L sheets for hybrid additive manufacturing applications. *J. Mater. Des. Appl.* **2021**, *235*, 2839–2850. [CrossRef]
15. Pérez-Ruiz, J.D.; de Lacalle, L.N.L.; Urbikain, G.; Pereira, O.; Martinez, S.; Bris, J. On the relationship between cutting forces and anisotropy features in the milling of LPBF Inconel 718 for near net shape parts. *Int. J. Mach. Tools Manuf.* **2021**, *170*, 103801. [CrossRef]
16. ASTM E8/E8 M. *Standard Test Methods for Tension Testing of Metallic Materials*; ASTM International: West Conshohocken, PA, USA, 2016.
17. Amini, S.; Gollo, A.H.; Paktinat, H. An investigation of conventional and ultrasonic-assisted incremental forming of annealed AA1050 sheet. *Int. J. Adv. Manuf. Technol.* **2017**, *90*, 1569–1578. [CrossRef]
18. Hill, R. A Theory of yielding and plastic flow of anisotropic metals. *Proc. R. Soc. Lond. Ser. A-Math. Phys. Sci.* **1948**, *193*, 281–297.
19. Marciniak, Z.; Duncan, J.L. *The Mechanics of Sheet Metal Forming*, 1st ed.; Edward Arnold: Auckland, New Zealand, 1992; pp. 100–113.
20. Martins, P.A.F.; Barata Marques, M.J.M. Plane strain rigid plastic finite element formulation for sheet metal forming processes. *J. Eng. Manuf.* **1993**, *207*, 167–171. [CrossRef]
21. Martins, P.A.F.; Bay, N.; Tekkaya, A.E.; Atkins, A.G. Characterization of fracture loci in metal forming. *Int. J. Mech. Sci.* **2014**, *83*, 112–123. [CrossRef]